Journal of Colloid and Interface Science 646 (2023) 872–882

Contents lists available at ScienceDirect

Journal of Colloid And Interface Science

journal homepage: www.elsevier.com/locate/jcis

Multi-dimensional plasmonic coupling system for efficient enrichment and ultrasensitive label-free SERS detection of bilirubin based on graphene oxide-Au nanostars and Au@Ag nanoparticles

Wenshi Zhao [a,b,c], Shuo Yang [d], Daxin Zhang [a,b,c], Tianxiang Zhou [a], Jie Huang [a], Ming Gao [a], Xiaolong Zhang [a], Yang Liu [a,*], Jinghai Yang [a,*]

[a] Key Laboratory of Functional Materials Physics and Chemistry of the Ministry of Education, Jilin Normal University, Changchun 130103, PR China
[b] Changchun Institute of Optics, Fine Mechanics and Physics, Chinese Academy of Sciences, Changchun 130033, PR China
[c] University of Chinese Academy of Sciences, Beijing 100049, PR China
[d] College of Science, Changchun University, Changchun 130022, PR China

HIGHLIGHTS

- SERS platform was designed by introducing secondary enhanced Au@Ag NPs on GO-AuNS.
- Multi-dimensional plasmonic coupling occurs in vertical and horizontal directions.
- SERS platform exhibits ultrasensitive SERS detection and enrichment capabilities.
- SERS platform has a linear SERS response and low detection limit of 10^{-11} M for BR.

GRAPHICAL ABSTRACT

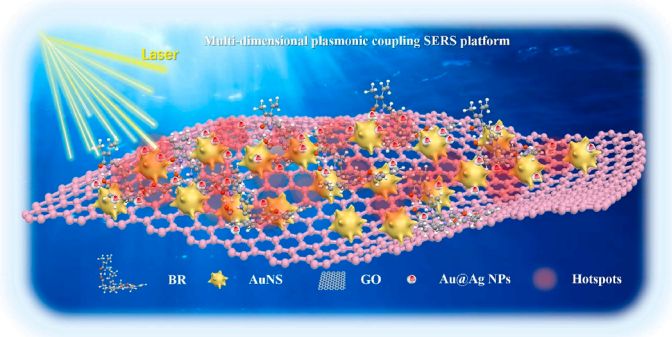

ARTICLE INFO

Keywords:
Surface-enhanced Raman scattering (SERS)
Graphene oxide-Au nanostars
Secondary reinforcing Au@Ag NPs
Multi-dimensional plasmonic coupling system
Bilirubin detection

ABSTRACT

Rapid and sensitive detection of free bilirubin (BR) is essential for early diagnosis of jaundice and other hepatobiliary diseases. Inspired by sandwich immunoassay strategy, a multi-dimensional plasmonic coupling SERS platform composed of graphene oxide-Au nanostars nanocomposites (GANS NCs) and Au@Ag nanoparticles (NPs) was designed for label-free detection of BR. Specifically, GANS NCs were first prepared, and their excellent SERS activity was ascribed to synergistic enhancement effect of electromagnetic enhancement and chemical enhancement. Furthermore, SERS spectroscopy was used to monitor the adsorption process of BR. Subsequently, secondary reinforcing Au@Ag NPs were directly added, ultimately resulting in a multi-dimensional plasmonic coupling effect. The SERS enhancing mechanism of coupled system was discussed through electromagnetic field simulations. Interestingly, the high-density hotspots generated by strong plasmonic coupling in GANS-Au@Ag substrate could lead to more extraordinary SERS enhancing behavior compared to GANS NCs. Sensing efficiency of the SERS platform was examined by BR with a detection limit down to 10^{-11} M. Besides, GANS-Au@Ag NCs performed high uniformity and reproducibility. This work not only opens up a new avenue for construction

* Corresponding authors.
E-mail addresses: liuyang@jlnu.edu.cn (Y. Liu), jhyang1@jlnu.edu.cn (J. Yang).

https://doi.org/10.1016/j.jcis.2023.05.117
Received 1 March 2023; Received in revised form 6 May 2023; Accepted 17 May 2023
Available online 22 May 2023
0021-9797/© 2023 Elsevier Inc. All rights reserved.

of multi-dimensional plasmonic coupling system, but also offers a new biosensing technology for label-free diagnosis of BR-related diseases, thereby expecting to be applied in clinical diagnosis.

1. Introduction

Bilirubin (BR) is a breakdown product of the hemoglobin formed during the heme metabolism of aged red blood cells, which can be divided into two types: conjugated BR and unconjugated BR [1,2]. Among them, unconjugated BR, also known as free BR, is found to be potentially toxic to humans [3]. In the blood circulation system, free BR can combine with glucuronic acid in the liver to form conjugated BR, which can be eventually excreted from body in the form of bile [4–6]. Nevertheless, newborns, especially preterm infants, have an elevated risk of hyperbilirubinemia owing to the over-production of BR, the insufficiency of BR transportation and the immature hepatic metabolic capacities of BR [7]. The free BR thus cannot be sufficiently eliminated and eventually accumulates in the body organs [8]. A dramatic rise in BR levels (>50 μM) and the resultant neonatal jaundice are inevitable, which will lead to permanent brain damage, biliary dysfunction, mental disturbance, respiratory system damage and even death [9]. Therefore, rapid and sensitive monitoring of the free BR concentration in human serum is crucial for early diagnosis of jaundice as well as other hepatobiliary diseases. To date, many methods, including direct spectroscopic measurement, diazo reaction method, electrochemical method and fluorescence method, have been developed for the accurate determination of free BR [6]. Although these types of methods have their respective merits, they have drawbacks such as time consumption, expensive instruments, low selectivity, high cost and low sensitivity.

As a surface-sensitive technology, surface-enhanced Raman scattering (SERS) has the strengths in terms of being easy to handle, cost-effective, highly accurate and sensitive, and compatible with small devices such as portable spectrometers [10–13]. Compared with the traditional biological detection technology, the biggest advantage of SERS is that it can directly provide inherent fingerprint information of bio-analytes in complex biological matrices without any modification or labeling [14]. As is known to all, SERS sensitivity can reach a signal enhancement factor of 10^{13}-10^{15} when the target analyte is adsorbed on or close to surfaces of SERS-active substrates [15]. In consideration of above advantages, SERS exhibits great potential in the field of BR detection [16]. At present, SERS signal enhancement can be explained by two main mechanisms: electromagnetic enhancement (EM) and chemical enhancement (CM) [17,18]. EM refers to the excitation of localized surface plasmon resonance (LSPR) excited by incident light on surfaces of noble metal nanostructures to generate a strong electromagnetic field. In order to improve SERS detection sensitivity, a favorite way is to design and construct noble metal-based nano-tip structures to create high-density hotspots [19]. It has been proved that anisotropic Au nanostars (AuNS) with multiple branches and rough surfaces feature have better SERS effects than spherical or rod-like nanostructures [20]. When the target molecule is located near the hotspots generated by the gaps or tips of AuNS, the SERS signals can be greatly enlarged due to LSPR coupling [21]. In view of above-mentioned reasons, AuNS have been widely regarded as the most promising SERS biosensing platform. In addition, because of the low concentration levels of biomolecules as well as weak interaction between biomolecules and Au nanoparticles (NPs), the sufficient adsorption of target molecules onto hotspots region is also another key point to improve SERS sensitivity.

It is generally accepted that two-dimensional layered graphene oxide (GO) has attracted great attention in SERS applications, which is attributed to its high specific surface area, good biocompatibility and chemical stability, and excellent molecular adsorption capacity [22]. Even though EM plays a principal role in the overall SERS enhancement, the contribution of CM in SERS enhancement effect is equally non-negligible [23,24]. Interestingly, GO can interact with various analytes through strong π-π coupling to promote efficient charge transfer, thus inducing additional CM [23]. As a result, it has become a research hotspot to detect BR by using GO as a loading platform of noble NPs, and has been reported by many researches. For example, Zou et al. developed a cellulose paper strip loaded with GO-isolated Au nanocrystals for detection of free BR [8]. Gao et al. constructed a GO/Ag SERS sensor to detect BR online [3]. Nevertheless, the combination of GO and AuNS for SERS detection of BR or even other cholochromes has received little attention. Furthermore, although the integration of GO and plasmonic AuNS can provide a powerful nanoplatform with dense SERS hotspots, the hotspots density requires to be further improved [25]. For generating maximum SERS enhancement, the construction of ultrasmall gaps is necessary, because more hotspots are not limited to forming in the horizontal plane but can be accurately engineered in the vertical direction [19]. Recently, the emerging strategy has turned to the multi-dimensional plasmonic coupling structures, which add secondary functional materials to introduce the plasmon coupling between adjacent nanoparticles, resulting in an increase in the density and intensity of SERS hotspots. Based on above idea, more complicated multi-dimensional plasmonic coupling SERS platforms formed by stacking GO with plasmonic noble metals have been investigated extensively. For instance, Liu et al. reported three-dimensional Ag NPs with multiple layers of GO as spacers to give rise to the strong plasmonic coupling in the vertical direction [26]. Liu and co-workers assembled a hyperbolic metamaterials/bilayer Ag NPs platform by using GO as a spacer layer and achieved highly sensitive SERS detection of adenosine molecules due to multiple plasmonic coupling effect [27]. Unfortunately, most currently reported SERS platforms are based on complex multilayer metal nanostructures, which usually require elaborate layer-by-layer assembly procedures. And the target molecules have difficulty entering the bottom hotspot region due to the steric hindrance. Therefore, it remains challenging to use new strategies to construct multi-dimensional plasmonic coupling structures with high-density hotspots and simple fabrication procedures.

Inspired by the sandwich immunoassay strategy which is a model that uses the formed “SERS active substrate-antibody-antigen–antibody-SERS active substrate” structure to double amplify the SERS signal of target antigen, a simple and original method has been proposed to realize multi-dimensional plasmonic coupling by dropping concentrated metal colloidal NPs on surfaces of SERS substrate-target complexes [28]. By sandwiching the analyte between two SERS substrates, the analyte molecules can be positioned at or near the center of the plasmonic SERS hotspots to achieve the final signal amplification. Among the numerous traditional single-metal colloidal NPs, Ag NPs exhibit the strongest plasmonic enhancement effect on SERS, while Au NPs have better surface stability than Ag NPs [29,30]. Combining these two metals to form a nanosized bimetallic core–shell structure can make full use of their respective advantages, which can not only solve the problem of stability, but also expand the excitation spectrum range and generate plasmon resonance coupling [31]. Nevertheless, the conventional SERS substrates such as GO-AuNS nanocomposites (GANS NCs) only can generate hotspots in the horizontal direction **(**Scheme 1**a)**. No researches, as we know, have been involved in the development of multiple coupling systems that combine GO-anisotropic nanostructures with secondary core–shell SERS enhancing substrates. More remarkably, there is no work focused on the enhancement of the SERS signal of bio-analytes by directly addition of secondary reinforcing substrates to form sandwich-like structures. Fortunately, our developed combinatorial SERS substrates (GANS-Au@Ag NCs) show strong electromagnetic field not only in the horizontal direction but also in vertical direction **(**Scheme 1**b)**. Moreover, the addition of Au@Ag colloidal NPs can promote

aggregation to further generate denser SERS hotspots [32]. Therefore, the combination of GANS NCs with Au@Ag NPs is expected to offer an unusual promising SERS platform to sensitively detect BR.

Herein, we proposed a novel SERS platform based on GANS NCs and secondary reinforcing Au@Ag core–shell NPs to realize multi-dimensional plasmonic coupling in GANS-Au@Ag substrate and achieve the ultrasensitive label-free SERS detection of BR. GANS NCs were first synthesized and served as a SERS active substrate, and then AuNS were assembled on surfaces of GO through electrostatic interactions. The signal enhancing capabilities of Au NPs, AuNS and GANS NCs were compared by choosing 4-mercaptobenzoic acid (4-MBA) as probe molecules. Meanwhile, EM and CM of GANS NCs were discussed respectively by combining finite-difference time-domain (FDTD) method and charge transfer model. Moreover, the adsorption kinetics of BR molecules on surfaces of GANS NCs was analyzed by simple SERS detection technology. To further enhance the SERS signal of BR, plasmonic Au@Ag NPs were chosen as secondary reinforcing SERS substrates. According to the electromagnetic field simulation and SERS detection results, SERS enhancement mechanism of multi-dimensional plasmonic coupling system was proposed and discussed. By integrating the high adsorption ability of GANS NCs and dual enhancement ability of GANS-Au@Ag SERS substrate, the formed multi-dimensional plasmonic coupling SERS platform achieved ultrasensitive label-free detection of BR molecules (10^{-11} M). This work is not only a continuation of the study of SERS enhancing mechanism of the multi-dimensional plasmonic coupling system, but also provides a novel biosensing platform for label-free ultrasensitive detection of BR with broad application prospects.

2. Materials and methods

The chemicals and instruments are listed in **Supplementary material**.

2.1. Assembly of GANS NCs

Firstly, GO was synthesized according to modified Hummer's method [33], and the detailed preparation procedure was described in **Supplementary material**.

The second step was the preparation of PVP and PDDA co-modified GO [34]. Specifically, 48 mg of PVP was poured into 12 mL of GO dispersion (0.5 mg/mL) and stirred overnight to prepare PVP-modified GO (GO-PVP). Subsequently, 1 mL of GO-PVP suspension (1 mg/mL) was added to 4 mL of the mixture that contained both KCl (187 mg) and PDDA (375 μL) and sonicated for 2 h. The products were centrifuged, and the obtained PDDA-modified GO (GO-PDDA) was redispersed in ultrapure water for later use.

The third step was the fabrication of GANS NCs [35]. Experimental details of Au NPs were described in our previous work [36]. And the specific synthesis process of AuNS was in **Supplementary material**. Under magnetic stirring, 160 μL of PDDA-GO was then poured into 3 mL of AuNS and sonicated for 2 min. Finally, after standing overnight, GANS NCs were obtained by centrifugation at 12000 rpm for 15 min.

2.2. Preparation of the secondary enhanced Au@Ag core–shell NPs

Au@Ag NPs were prepared in two steps [37]. The first step was to prepare Au NPs following the standard sodium citrate reduction method used in our previous work [36]. The second step was to prepare Au@Ag NPs by reducing Ag shell on surface of Au core. Briefly, 25 mL of Au NPs was diluted to 100 mL with ultrapure water and heated to boiling. Subsequently, 2.5 mL of $AgNO_3$ solution (1.6 mg/mL) was added under vigorous stirring. Ultimately, 1.5 mL of 1% sodium citrate solution was poured dropwise into above solution as a reducing agent, and reaction was kept at 85 °C for 40 min until the color of solution varied from wine red to yellow to obtain Au@Ag NPs.

2.3. SERS detection of BR

For SERS detection of BR, BR powder was configured into various concentrations of BR solution ranging from 10^{-4} M to 10^{-12} M using PBS buffer. Then, 500 μL of BR solution was mixed with 100 μL of 1 mg/mL GANS NCs, respectively. After incubation for 55 min, the obtained complexes were centrifuged and washed, and then resuspended in 10 μL of PBS buffer and dropped on an aluminum pan plate (No. 0219-0041, Perkin-Elmer, Waltham, MA, USA). Subsequently, 20 μL of concentrated Au@Ag NPs was dropped on aluminum pan plate. After droplet evaporated completely, the SERS signal was recorded by the Raman microscope system.

3. Results and discussion

3.1. Formation mechanism and structural characterization of GANS NCs

Schematic drawing for synthesis process of GANS NCs is shown in Fig. 1**a**. The main formation steps of GANS NCs are to functionalize GO with PVP and PDDA sequentially, and then self-assemble AuNS onto surfaces of the modified GO. The microscopic morphologies of as-obtained GO, AuNS and GANS NCs were visualized through TEM and SEM. As shown in Fig. 1**b1** and Fig. 1**c1**, GO reveals the 2D layered structure with various degrees of wrinkles. The observed wrinkles of GO can provide abundant adsorption active sites for AuNS [25]. As exhibited in Fig. 1**b2** and Fig. 1**c2**, AuNS are composed of a central core with a diameter of about 85 nm and many multiple sharp and irregular branches with the average length of 15 nm. The special morphology of AuNS is closely related to their preparation process. First, Au NPs were synthesized by sodium citrate reduction method, which were served as core seeds. Then, sodium citrate and hydroquinone (the growth

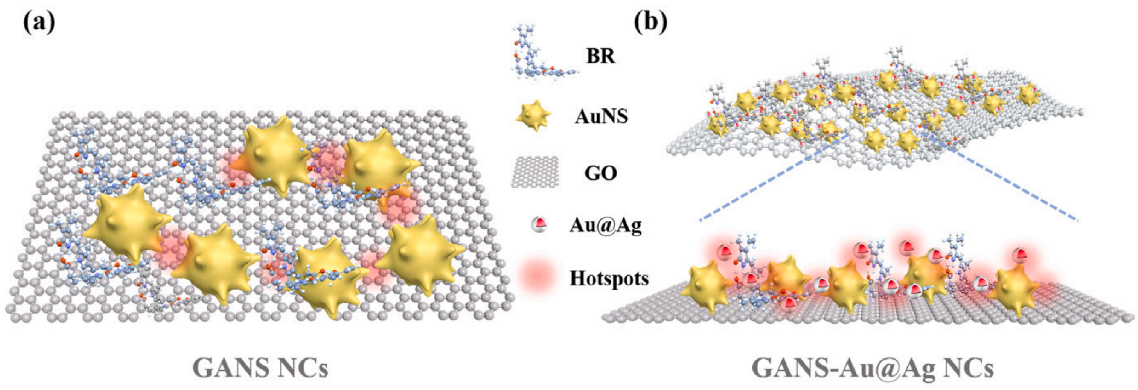

Scheme 1. (a) Conventional SERS platform (GANS NCs), (b) the novel SERS platform proposed in this work (GANS-Au@Ag NCs).

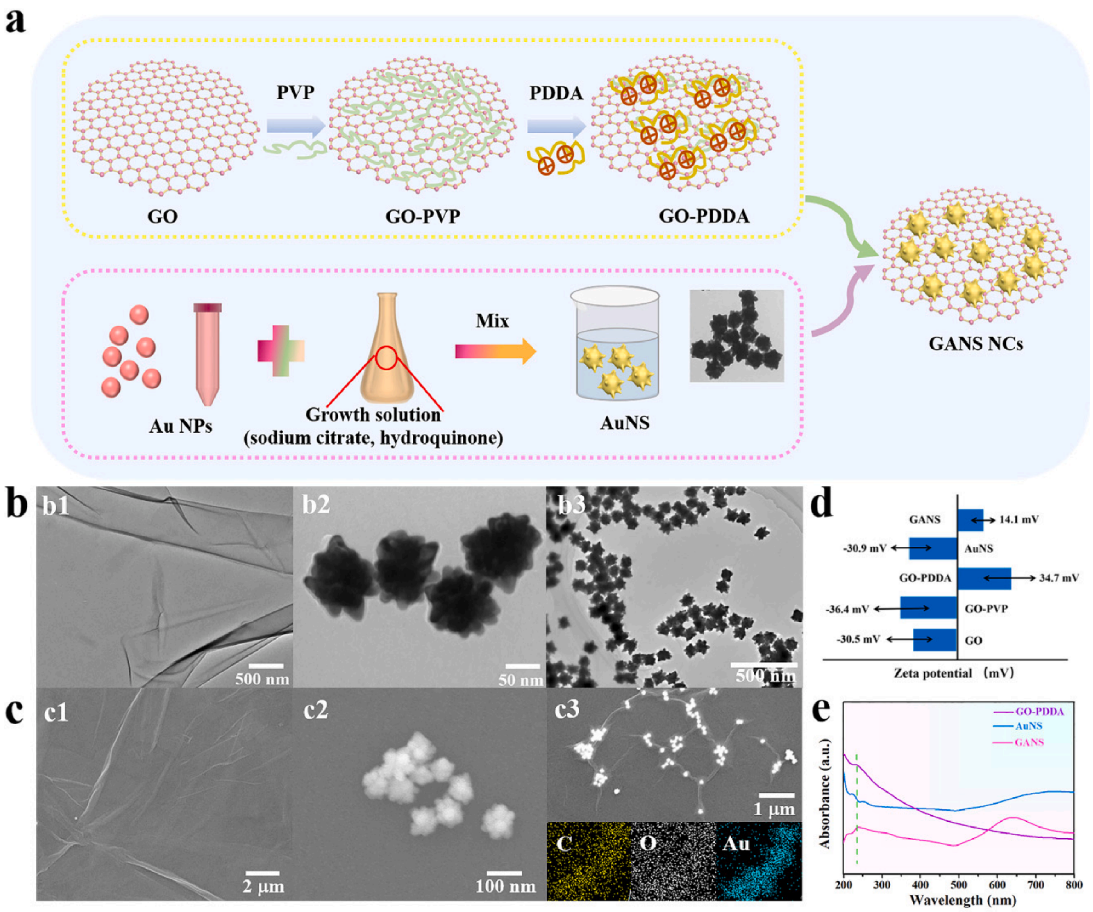

Fig. 1. (a) Schematic drawing of fabrication process of GANS NCs, (b) TEM images of (b1) GO, (b2) AuNS and (b3) GANS NCs, (c) SEM images of (c1) GO and (c2) AuNS, (c3) SEM image and EDS elemental mapping images of GANS NCs (C, O and Au), (d) zeta potential characterization of GO, GO-PVP, GO-PDDA, AuNS and GANS NCs and (e) UV–Vis spectra of GO-PDDA, AuNS and GANS NCs.

solution) were both used as reducing agents [38]. In the reaction system, sodium citrate with weak reducing ability can reduce Au^{3+} to Au^{1+}, and hydroquinone with strong reduction ability further reduces Au^{1+} to Au^{0} [35]. In this process, hydroquinone can highly and selectively reduce Au^{1+}, which contributes to anisotropic growth of NPs and ultimately leads to form irregular tip branches [39]. As for GANS NCs, AuNS are loaded on the surfaces of GO, which can be verified by the TEM image in Fig. 1**b3** and SEM image and EDS elemental mapping images in Fig. 1**c3**. AFM images further exhibited the structural details of GO and GANS NCs. As presented in Fig. S1**a**, GO exhibits a thin layer structure with smooth surfaces. Many bright spots observed in AFM image of GANS NCs (Fig. S1**b**) indicate the successful loading of AuNS on GO surfaces. In addition, the size distribution diagram in the inset of Fig. S1**a** and Fig. S1**b** shows that the average thickness of GO and GANS increases from 2.9 to 100.2 nm, which is consistent with the results of TEM and SEM. The zeta potentials of GO, GO-PVP, GO-PDDA, AuNS and GANS NCs were tested to understand the self-assembly and formation mechanism of GANS NCs. As reflected in Fig. 1**d**, the abundant carboxyl and hydroxyl functional groups on surfaces of GO make it carry negative charges, and the change of zeta potential from −30.5 mV (GO) to −36.4 mV (GO-PVP) demonstrates that the modification of amphiphilic PVP molecule let GO more negative charged [40]. Once the surfaces of GO-PVP are further modified with positively charged PDDA by electrostatic attraction, a significant shift in zeta potential value from negative to positive (+34.7 mV) is observed. Because of the strong electrostatic interactions, the negatively charged AuNS (-30.9 mV) are assembled on surfaces of positively charged GO-PDDA and the obtained GANS NCs have a zeta potential value of +14.1 mV. Additionally, UV–Vis spectra were used to study optical properties of GO-PDDA, AuNS and GANS NCs. As depicted in Fig. 1**e**, an obvious absorption peak at 230 nm can be observed in both GO-PDDA and GANS NCs, corresponding to π-π* electronic transition of GO. AuNS generate a broad LSPR absorption band ranging from 500 to 800 nm, and broadening of the LSPR bandwidth is owing to the difference in branch length of AuNS [41]. After the formation of GANS NCs, the LSPR peak position shows a blue shift compared with that of AuNS. This may be because of the electronic interaction between GO and AuNS and change in dielectric constant [9,42]. The crystallographic structures of GO and GANS NCs were then analyzed by XRD. Fig. S2**a** presents that the characteristic peak (0 0 1) of GO is observed around $2\theta = 11.02°$. After depositing AuNS on GO, four new diffraction peaks are appeared at 38.24°, 44.47°, 64.85° and 77.86°, which can be indexed to (1 1 1), (2 0 0), (2 2 0) and (3 1 1) planes of face-centered-cubic structure Au (JCPDS No. 04-0748), respectively [43]. Furthermore, XPS was further applied to characterize the chemical composition of GO and GANS NCs. It can be seen from Fig. S2**b** that compared with GO, the additional Au *4f* signal is appeared in the XPS spectrum of GANS NCs. The high resolution XPS spectrum of Au *4f* for GANS NCs in Fig. S2**c** shows two peaks at 85.25 eV and 86.85 eV, corresponding to the Au $4f_{7/2}$ and Au $4f_{5/2}$ core levels of metallic Au, respectively [44]. Therefore, the above results all confirm the successful preparation of GANS NCs.

3.2. SERS activity and enhancement mechanism of GANS SERS substrate

To evaluate the SERS signal amplification and fingerprinting capability of GANS NCs, 4-MBA was used as a probe molecule for SERS

detection. SERS spectra of 4-MBA (10^{-4} M) absorbed on Au NPs, AuNS and GANS NCs are shown in Fig. 2**a**. Four SERS bands at 1078, 1185, 1490 and 1589 cm^{-1} are observed from SERS spectra. Notably, SERS spectra of 4-MBA on AuNS and GANS NCs are slightly different in SERS peak positions after comparison. Once AuNS are assembled on the surfaces of GO, three new SERS peaks are found at 1014, 1145 and 1398 cm^{-1} due to the interaction between 4-MBA and GANS SERS substrate. It is universally acknowledged that SERS peaks of 4-MBA mainly consist of two vibrational modes including symmetric (a_1) and asymmetric modes (b_2), where the enhancement of vibrational mode is ascribed to charge transfer process occurring between 4-MBA molecules and SERS substrates [29]. **Table S1** exhibits the detailed SERS band assignments of 4-MBA molecules. The corresponding SERS intensities of 4-MBA on three different substrates at 1589 cm^{-1} are presented in Fig. 2**b**. The testing results clearly show that SERS intensity of 4-MBA on AuNS substrate is stronger than that on Au NPs. It is remarkable that SERS enhancement ability of GANS NCs is remarkable higher than that of bare AuNS, indicating that the contribution of CE effect of GO is not insignificantly. For better estimating the performance of SERS substrates, the SERS enhancement factor (EF) was calculated. Figure S3 shows Raman spectrum of pure 4-MBA molecules. EF value of GANS NCs is calculated to be approximately 4.7×10^7, and is higher than that of Au NPs (5.59×10^6) and AuNS (1.85×10^7). Detailed calculation of EF is provided in Supplementary material. A possible SERS enhancement mechanism was put forward based on above results. Given that the extensive recognized SERS enhancement mechanism focuses on EM and CM, the roles of the two mechanisms in the significant SERS enhancing behavior of GANS NCs were discussed. Among them, EM mechanism, which plays a primary role in SERS enhancing behavior, mainly originates from the excitation of LSPR generated on surfaces of noble metal NPs [45]. The local electromagnetic field intensity distribution between adjacent AuNS was simulated by FDTD simulation, as revealed in Fig. 2**c1**. It is obvious that the tips of AuNS produce high localized electric field enhancement, while the stronger electromagnetic field is produced in narrow particle gaps between AuNS. In short, the sharp tip structure and nanogap between tips lead to the most efficient field enhancement, so it is plausible that AuNS and GANS NCs generate better SERS enhancement effect of 4-MBA than Au NPs. Additionally, unlike EM, the

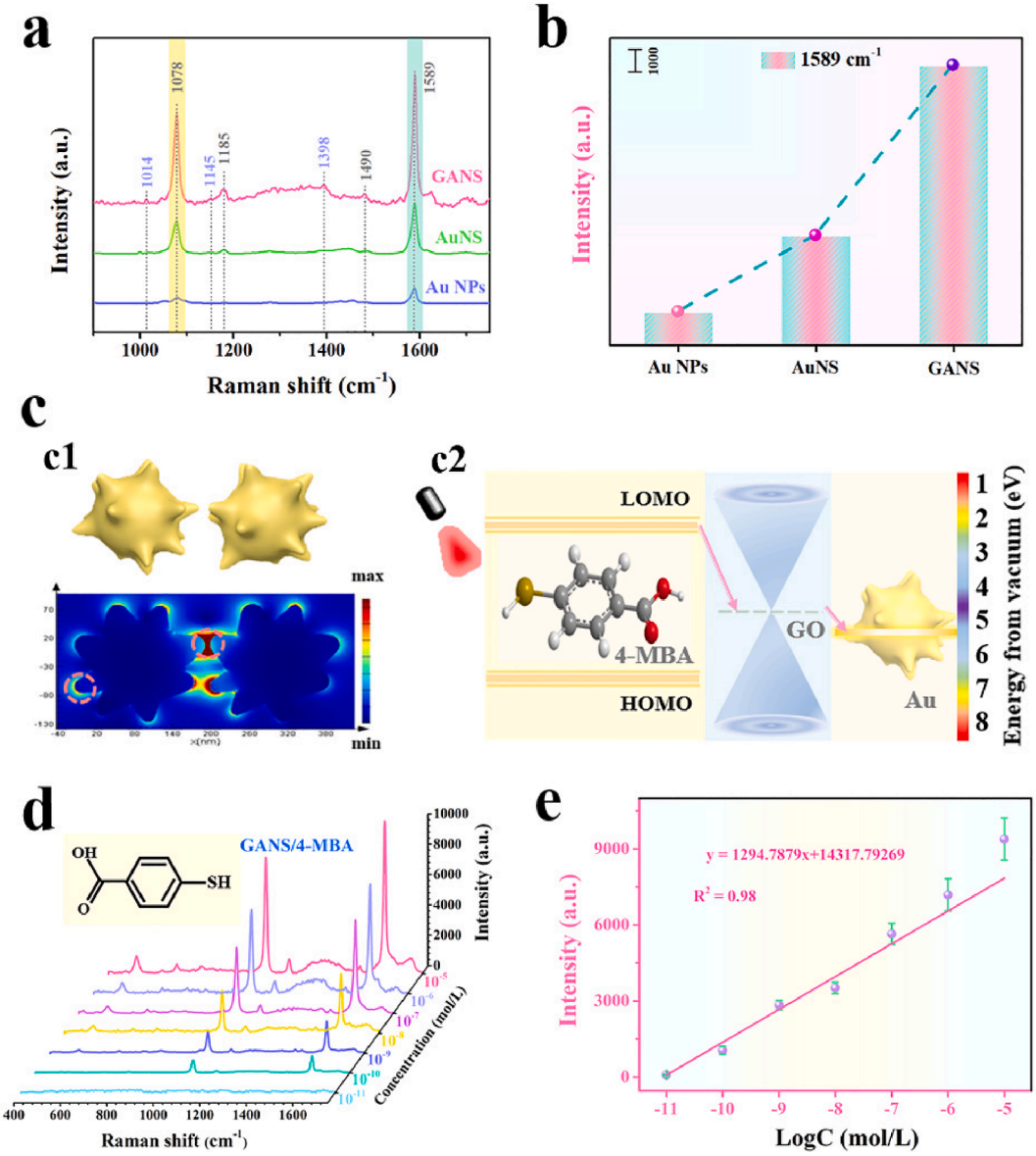

Fig. 2. (a) SERS spectra and (b) SERS intensities of 4-MBA at 1589 cm^{-1} on Au NPs, AuNS and GANS NCs, (c) (c1) electric field distribution of adjacent AuNS and (c2) the schematic diagram of charger transfer process between GANS NCs and 4-MBA molecules, (d) SERS spectra of 4-MBA (10^{-5}-10^{-11} M) on GANS SERS substrate and (e) the linear correlation of logarithm of 4-MBA concentration versus SERS intensity at 1589 cm^{-1}.

contribution of CM in SERS enhancement is through charge transfer between SERS substrates and adsorbed target molecules [14]. This is because the above-mentioned charge transfer process will enhance the electron–phonon coupling, thereby resulting in additional SERS signal enhancement. As a zero-bandgap semiconductor, GO can enhance Raman scattering of target molecules, which is mainly achieved by the ground-state chemical interaction between π-electron and absorbed molecules. Therefore, GANS NCs can emerge stronger SERS signals than single AuNS due to their non-negligible CM contribution to SERS enhancement. To further investigate the CM mechanism of GANS NCs, a possible interfacial charge transfer process was also proposed, as illustrated in Fig. 2**c2**. On one hand, the electrostatic attraction and π-π stacking interaction between negatively charged 4-MBA (**Figure S4**) and GANS NCs form the stable bond, 4-MBA was close to SERS substrate, thus promoting the charge transfer between them [46]. On the other hand, since work function of GO (4.6–4.9 eV) is located between the HOMO energy level (6.24 eV) and the LUMO (1.68 eV) energy level of 4-MBA, which is slightly less than that of Au (5.14 eV), the electrons transferred to GO can be further transferred to Au and this process also enables Au to obtain higher electromagnetic enhancement [46,47]. Moreover, charge transfer process can also enhance and enlarge the polarizability and Raman scattering cross section of 4-MBA to amplify the SERS signal [48]. Furthermore, to examine the interaction between the Raman substrates and adsorbate molecules, the UV–Vis spectra of 4-MBA before and after deposition on GANS NCs were collected. As shown in **Figure S5**, the bands at 200–300 nm are the characteristic absorption peak of 4-MBA solution. For the GANS/4-MBA, the peak red-shifts compared with pure 4-MBA, indicating the occurrence of the charge transfer between GANS NCs and 4-MBA. In conclusion, from the perspective of EM and CM, SERS enhancement of GANS substrate is jointly contributed by EM and CM. The significant SERS enhancing performance of GANS substrate is mainly explained by the following factors: (i) the tip hotspots effect of AuNS; (ii) the extremely intense EM field concentrated in the narrow nanogaps between adjacent AuNS assembled on surfaces of GO and (iii) the additional CM and stronger EM realized by charge transfer between GANS NCs and molecules.

Afterward, SERS detection on different concentrations of 4-MBA (10^{-5} to 10^{-11}) was performed by using GANS NCs. SERS signal intensity of 4-MBA decreases with the decrease of concentration, as depicted in Fig. 2**d**. The limit of detection (LOD) of 4-MBA absorbed on GANS NCs is 10^{-10} M, which is lower than that of similar plasmonic hybrid SERS substrates reported previously [49,50]. A strong linear correlation between SERS intensity and logarithm of 4-MBA concentration ($y = 1294.7879\ x + 14317.79269$, $R^2 = 0.98$) can be observed (Fig. 2**e**), which indicates that the prepared GANS SERS substrate can be used for quantitative analysis of unknown concentrations of 4-MBA.

3.3. Adsorption kinetics and SERS detection of BR

As aforementioned, GANS SERS substrate has the excellent SERS enhancement effect on negatively charged molecules with aromatic structure. In view of the characteristics of BR, including negative charge on the surfaces (**Figure S6**) and the strong π-π interaction with GO, the developed SERS substrate is suitable for the potential application of highly sensitive SERS detection of BR. Because of the fact that the good absorption capability of SERS substrate to target analytes affects the sensitivity of SERS detection, it is necessary to study the adsorption capacity of the SERS substrate to BR in order to further explore the label-free SERS detection of BR [51]. Since SERS intensity is correlated to adsorption properties and adsorption time of SERS substrate to target analytes, the time-resolved SERS spectroscopy method was applied to monitor the whole adsorption process. In this process, GANS SERS substrate with excellent SERS performance was used to detect BR. SERS spectra were measured at various incubation times to comprehend the adsorption kinetics of BR on GANS NCs. Characteristic SERS peaks of BR molecules can be clearly observed in Fig. 3**a**, and the specific assignment of SERS modes is recorded in **Table S2** [4,52,53]. In Fig. 3**b**, SERS intensity of BR increases with the rising incubation time and then reaches saturation. SERS response, which is so-called as SERS intensity ratio (I/I_{max}), was taken as an index for absorption process. I_{max} is the maximum SERS intensity at 1614 cm^{-1} [9]. By simulating the relationship of time as well as SERS response, it can be observed that adsorption data of BR

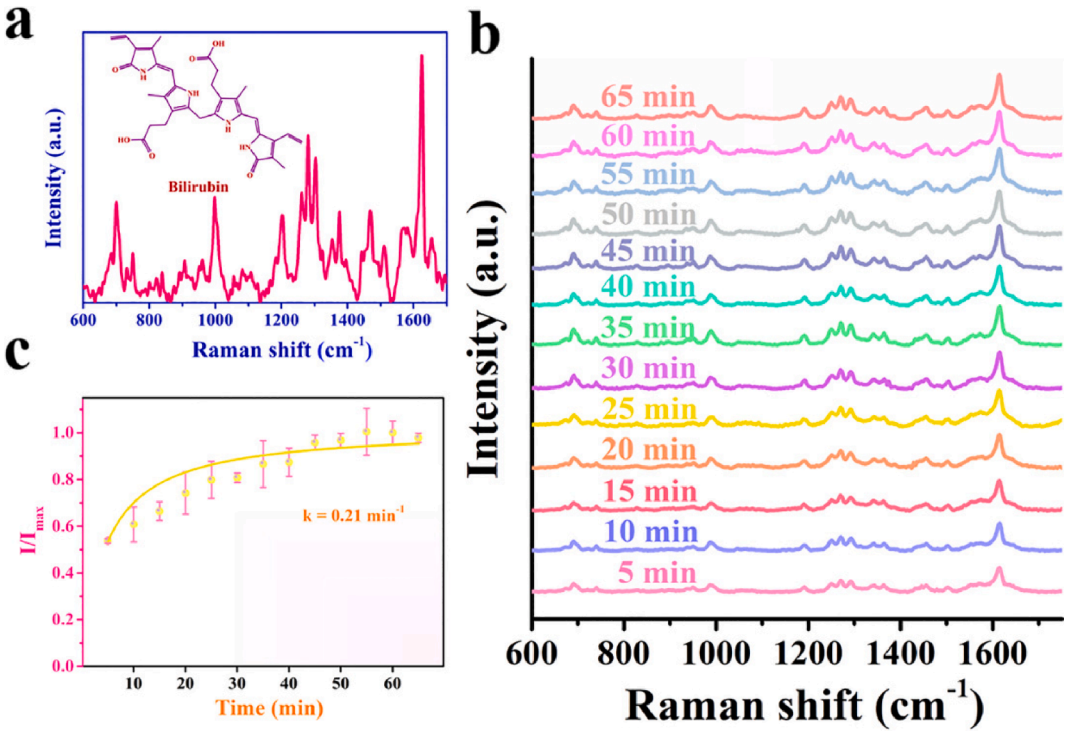

Fig. 3. (a) Molecular structure and SERS spectrum of BR (10^{-4} M), (b) evolution of SERS spectrum of BR over time (from 5 min to 65 min), (c) adsorption kinetic curves of GANS NCs toward BR molecules.

($q_t = I/I_{max}$) follows pseudo-second-order kinetic model [54]:

$$q_t = \frac{q_e^2 kt}{1 + q_e kt} \quad (2)$$

where q_e and q_t represent adsorption amount at equilibrium and time t, and k is adsorption rate constant of pseudo-second-order kinetic model. Adsorption kinetics reflects that the adsorption of BR molecules by GANS NCs reaches equilibrium within 55 min (Fig. 3**c**), thus identifying the optimal adsorption time for BR in the subsequent experiments. Additionally, the fitting parameter values of absorption capacity and adsorption rate constant are estimated to be 1010 mg/g and 0.21 min^{-1}, respectively. Compared with many previous literatures [55–57], GANS NCs have stronger absorption capability to BR, which may be attributed to strong π-π interactions between GO and tetrapyrrole rings of BR, and the strong electrostatic interaction between BR containing carboxyl functional groups and GANS with cationic PDDA surface ligands. The π-π interactions and the electrostatic interaction can enrich the molecules to SERS hotspots, and thus result in the excellent SERS enhancement ability of GANS NCs. To further assess the SERS detection sensitivity of GANS NCs for biosensing application, SERS spectra of BR solution with concentrations of 10^{-4} M–10^{-9} M loaded on GANS NCs were collected (**Figure S7**). The results suggest that the as-prepared GANS NCs exhibit high sensitivity, and LOD of BR reaches down to 10^{-8} M. However, although the combination of GO and AuNS can achieve a significant enhancement of local electromagnetic field, the plasmonic coupling is limited by the structure and only happens in the horizontal direction (Scheme 1**a**). To further enhance SERS sensitivity, it is essential to construct the additional plasmonic coupling in vertical direction by introducing the secondary reinforcing NPs to generate hotspots with higher density (Scheme 1**b**).

3.4. Characterization of the secondary enhanced Au@Ag NPs

As mentioned above, in recent years, novel SERS substrates combining two noble metals into one system have attracted extensive attention. As one of the most important bimetallic NPs, Au@Ag NPs combine the extraordinary structural stability of Au NPs and the superior SERS signal enhancement ability of Ag NPs, which are universally recognized as ideal nanomaterials for the secondary enhancement of SERS signals [58,59]. The morphologies of Au and Au@Ag NPs were analyzed via TEM. As observed from Fig. 4**a**, Au NPs with the average diameter of 15 nm show regular spherical morphology and homogeneous dispersion. As presented in Fig. 4**b**, TEM picture of Au@Ag NPs, by contrast, clearly suggests that Au NPs are coated with uniform Ag shells (~3 nm in thickness). UV–Vis spectra of Au and Au@Ag NPs are demonstrated in Fig. 4**c**. Au NPs exhibit a sharp LSPR peak at about 520 nm. Differing from Au NPs, Au@Ag NPs display two strong absorption bands centered near 395 nm and 500 nm and a weak band near ~320 nm. Peaks located at ~ 395 and ~320 nm are attributed to the characteristic peak of Ag shell and the dielectric properties of Ag NPs, respectively [60]. Meanwhile, owing to the diverse surface plasmon resonance frequencies of Au NPs as well as Au@Ag NPs, the absorption peak of Au NPs has a slight blue shift after Ag shell coating [61]. Additionally, to contrast SERS enhancement ability of Au and Au@Ag NPs, we performed SERS measurements on BR solution (10^{-4} M) under 632.8 nm laser, respectively. Obviously, as presented in Fig. 4**d**, Au@Ag NPs show a better SERS enhancement performance compared with Au NPs, which demonstrates that Au@Ag NPs can be served as secondary reinforcing substrates to realize secondary enhancement of SERS signals for BR molecules.

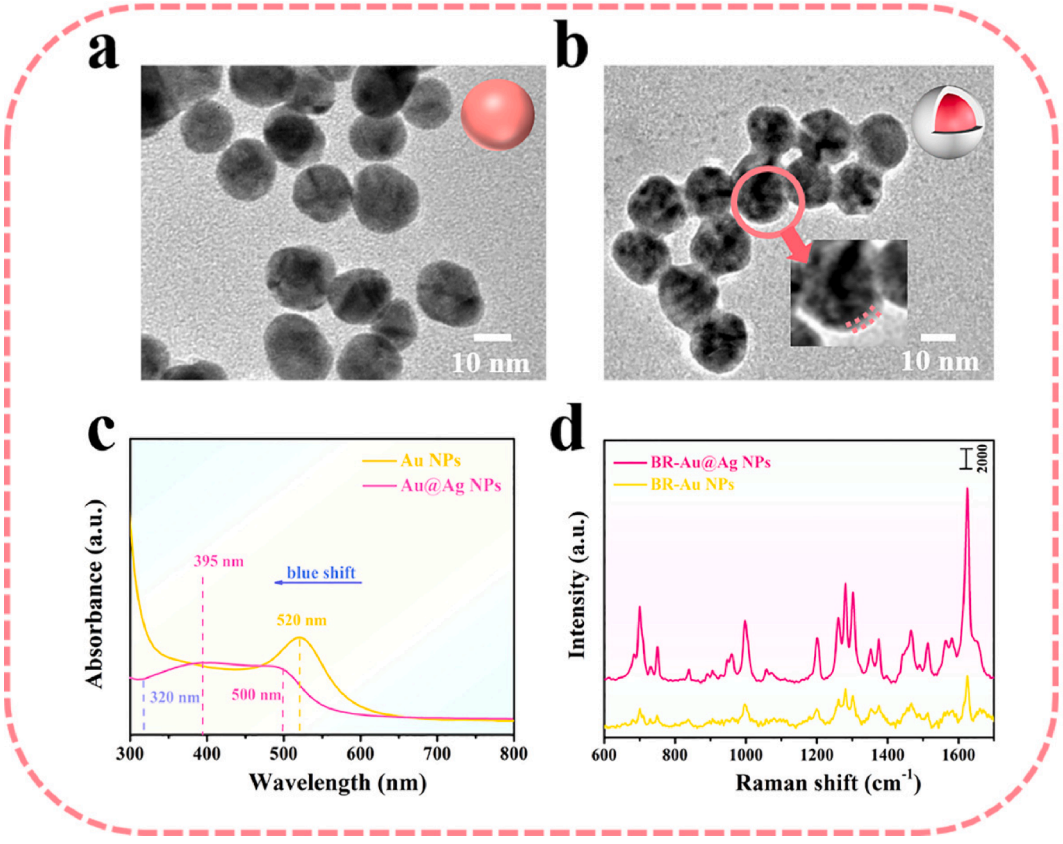

Fig. 4. TEM images of (a) Au NPs and (b) Au@Ag NPs, (c) UV–Vis spectra of Au NPs and Au@Ag NPs, (d) SERS spectra of BR molecules on Au NPs and Au@Ag NPs.

3.5. SERS enhancement mechanism of multi-dimensional plasmonic coupling system

Fig. 5**a** represents the schematic diagram for label-free SERS detection of BR by multi-dimensional plasmonic coupling SERS platform. Inspired by the sandwich immunoassay strategy with the structure of "SERS active substrate-antibody-antigen–antibody-SERS active substrate", our designed SERS platform constructs the sandwich structure of GANS-BR-Au@Ag complexes. Firstly, GANS NCs were incubated with BR molecules for 55 min. The π-π interactions and strong electrostatic interaction allow GANS NCs to enrich more BR molecules, and GANS NCs with a large number of hotspots are conducive to the SERS signal enhancement of BR [3]. Secondly, GANS-BR complexes were collected by centrifugation and transferred to precleaned aluminum pan plate. Afterward, the concentrated Au@Ag NPs were added to GANS-BR complexes to form GANS-BR-Au@Ag complexes for SERS detection. In this manner, Au@Ag NPs can diffuse into the GANS-BR complexes and eventually form ultrasmall gaps between Au@Ag NPs and AuNS tips and between adjacent Au@Ag NPs, as shown in the model in Fig. 5**b**. To further verify that the multi-dimensional coupling enhancement strategy has the strongest signal amplification effect, the SERS spectra of 4-MBA and BR on GANS and GANS-Au@Ag SERS substrates were compared, respectively. As demonstrated in **Figure S8** and Fig. 5**c**, SERS signal intensity of 4-MBA and BR molecules absorbed on the GANS-Au@Ag SERS substrate is much higher than that absorbed on GANS, which proves that simply mixing GANS NCs and Au@Ag NPs can lead to more superior SERS enhancement. Meanwhile, it is calculated that EF value of GANS-Au@Ag SERS substrate is as high as 1.2×10^8 (the detailed calculation process is described in **Supplementary material**), which is 2.6 times that of GANS NCs (4.7×10^7). Furthermore, to gain a better understanding of how the multiple plasmonic resonance coupling achieves excellent SERS enhancement, the electromagnetic field distributions of Au@Ag and GANS-Au@Ag substrates were simulated using FDTD method. The simulation result in Fig. 5**d** shows that tremendous hotspots are generated in the nanogaps between Au@Ag NPs because of the electromagnetic field coupling effect. As for GANS-Au@Ag NCs, the more hotspots distribution can be observed from Fig. 5**e**. On one hand, strong coupling occurs between the high-density AuNS assembled on surfaces of GO, thus generating highly enhanced electromagnetic field in the nanogaps between AuNS as well as at the tips of AuNS. On the other hand, the LSPR coupling between Au@Ag NPs induces an enhancing electromagnetic field in interparticle gaps. Finally, multi-dimensional plasmonic coupling is stimulated between the anisotropic AuNS and the closely spaced Au@Ag NPs in both horizontal and vertical directions, thereby enhancing the density of hotspots to further provide a huge electromagnetic enhancement. As mentioned above, the following conclusions can be drawn that the enormous SERS enhancing behavior of GANS-Au@Ag NCs benefits from the high-density hotspots generated by the strong plasmonic coupling in the hybrid system, mainly including the tip-to-tip plasmonic coupling of AuNS, interparticle coupling between horizontally AuNS with narrow nanogaps on surfaces of GO, the LSPR effect between the adjacent Au@Ag NPs and the plasmonic coupling between GANS NCs and Au@Ag NPs in both horizontal and vertical directions. Moreover, GO not only can concentrate BR within hotspots due to its superior enrichment ability, but also generate CE contribution through charge transfer resonance with BR, which also can enhance the SERS signals to a certain extent. From another perspective, in addition to hotspots density, hotspots types also influence SERS sensitivity to a large extent [62]. Differences in morphology can cause different types of hotspots, and the simple hybrid assembly of the two nanostructures of GANS NCs and Au@Ag NPs can simultaneously generate three types of hotspots, including tip-to-tip hotspots (GANS NCs), point-to-point hotspots (Au@Ag NPs) and tip-to-point hotspots (GANS-Au@Ag), resulting in exceptionally strong electric field enhancement.

3.6. SERS detection of BR assisted by multi-dimensional plasmonic coupling system

The highly accurate and sensitive SERS platform based on multi-dimensional plasmonic coupling system was used to detect BR molecules. SERS spectra of BR molecules with concentrations of 10^{-4} to 10^{-12} M absorbed on GANS-Au@Ag NCs are exhibited in Fig. 6**a**. As can be observed when BR concentration decreases from 10^{-4} to 10^{-11} M, SERS intensity gradually decreases. The LOD of SERS platform for BR can be down to 10^{-11} M. SERS spectrum peak at 1614 cm^{-1} was used for quantitative analysis of BR. A strong linear correlation between logarithm of BR concentration and SERS intensity (y = 4065.5 x + 46166.5,

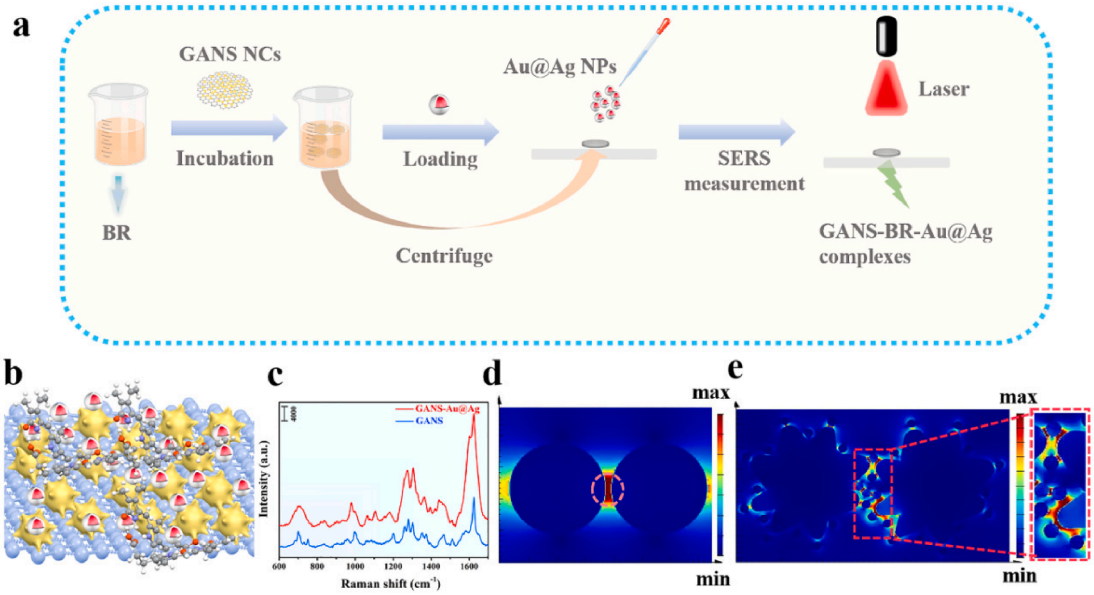

Fig. 5. (a) Schematic diagram for SERS-based label-free detection of BR by using GANS combined with Au@Ag NPs, (b) simulation configuration of GANS-BR-Au@Ag, (c) SERS spectra of BR adsorbed on GANS and GANS-Au@Ag SERS substrate under the same conditions, electric field distributions of (d) Au@Ag NPs and (e) GANS-Au@Ag NCs.

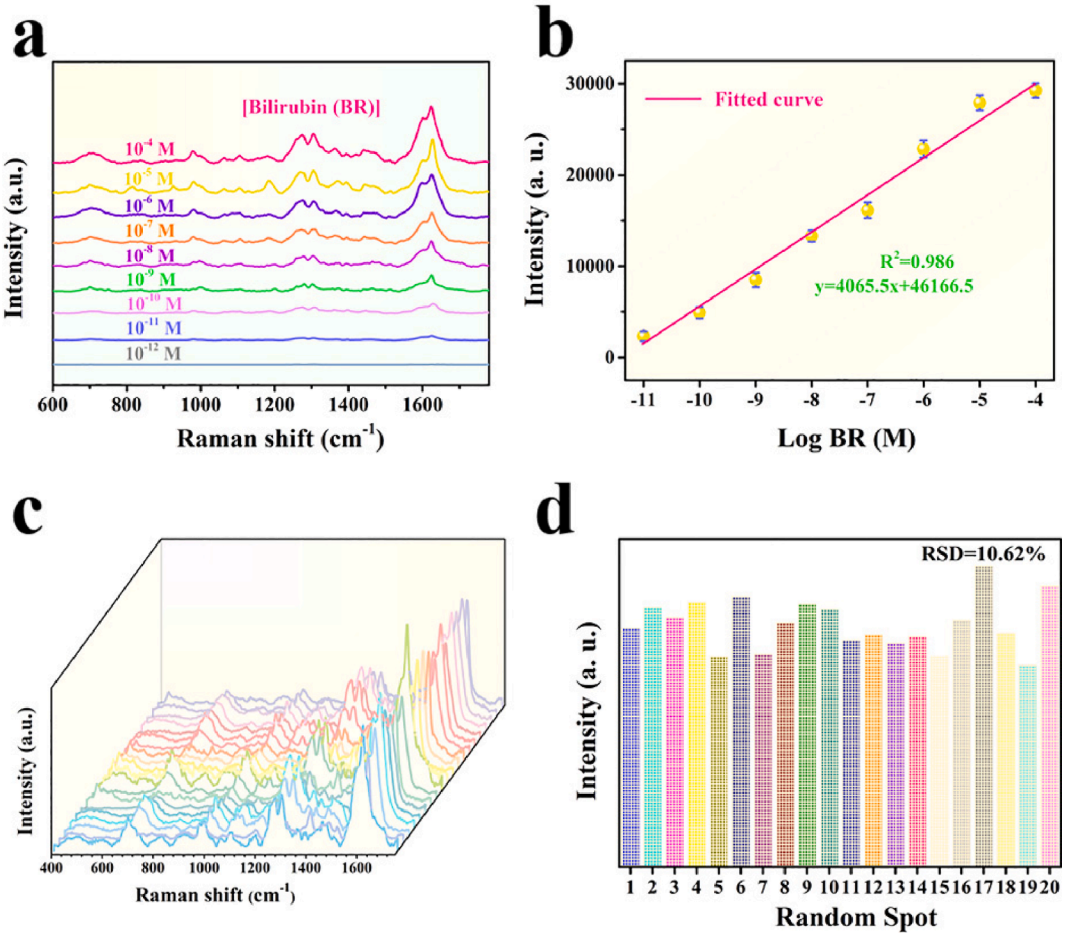

Fig. 6. SERS spectra recorded from GANS-Au@Ag substrate for BR with various concentrations ranging from 10^{-4} to 10^{-12} M, (b) linear correlation between logarithm of BR concentration and SERS intensity at 1614 cm^{-1}, (c) SERS spectra of BR recorded from 20 random spots on GANS-Au@Ag NCs and (d) SERS intensities of BR at 1614 cm^{-1} of 20 SERS spectra.

R^2 = 0.986) can be observed from Fig. 6**b**, which indicates that our method has a good ability in quantitatively detect BR molecules in a wide range. Compared with other diverse analytical techniques for detecting BR, as recorded in Table 1 [1,5,7,16,63,64], our as-proposed SERS platform exhibits the highest SERS sensitively. Moreover, besides highly SERS sensitivity, good uniformity and reproducibility are equally significant for SERS substrate. We further verified the uniformity of SERS signal based on the SERS platform by randomly selecting 20 different points from 10^{-6} M BR solution. It can be seen from Fig. 6**c and 6d** that SERS signal intensity distribution at 1614 cm^{-1} is highly uniform and relative standard deviation (RSD) value is 10.62%. Furthermore, we randomly selected 15 batches of GANS NCs and Au@Ag NPs to study the batch-to-batch reproducibility. SERS spectra of BR with the concentration of 10^{-6} M adsorbed on GANS-Au@Ag NCs and the corresponding SERS intensities at 1614 cm^{-1} are shown in **Figure S9a and S9b**. The RSD value of signal intensity is 9.07%. All of the above results demonstrate that our SERS platform has ultrahigh sensitivity, excellent uniformity and reproducibility.

Table 1
LOD on the GANS-Au@Ag SERS substrate in comparison with other analytical methods for BR detection.

Detection method	Substrates	Linear range (M)	LOD (M)	Reference
SERS	Ag@Fe_2O_3	5×10^{-8} to 1×10^{-4}	2.3×10^{-8}	[1]
SERS	Ag NRs/M-BN	5×10^{-8} to 1×10^{-4}	1.4×10^{-8}	[7]
Fluorescent	UiO-66$(COOH)_2$Zr-MOF: Eu^{3+}	0 to 1.5×10^{-5}	4.5×10^{-7}	[63]
SERS	MoS_2@ZnO@Ag	10^{-8} to 10^{-3}	10^{-8}	[16]
Electrochemical	Ceria nanocubes	10^{-6} to 10^{-4}	10^{-7}	[64]
SERS	Glucose-Au array substrate	10^{-10} to 10^{-5}	10^{-10}	[5]
SERS	GANS-Au@Ag	10^{-11} to 10^{-4}	10^{-11}	this work

4. Conclusions

In conclusion, a multi-dimensional plasmonic coupling SERS platform composed of GANS NCs and Au@Ag NPs has been developed and applied to the ultrasensitive detection of BR. GANS NCs were prepared successfully and the corresponding formation mechanism was discussed. After comparing SERS enhancing performance of Au NPs, AuNS and GANS NCs using 4-MBA as reporter molecule, it was found that the combination of GO and AuNS had the most excellent SERS performance, which attributed to the huge hotspots formed between AuNS on GO surfaces and the additional CM induced by GO during the charge transfer process. In addition, the adsorption process of BR on GANS NCs was monitored by SERS spectroscopy. Results illustrated that the adsorption process was accorded with the pseudo-second-order kinetic model with a time of 55 min until adsorption equilibrium, and the GANS NCs had good adsorption capacity for BR owing to π-π interactions and electrostatic interaction. Combining Au@Ag NPs as secondary reinforcing SERS substrates with GANS NCs was used to construct a novel

multi-dimensional plasmonic coupling system. The SERS platform had a superior SERS sensitivity with a low LOD of 10^{-11} M, and SERS peak intensity and logarithm of BR concentration from 10^{-4} to 10^{-11} M showed a strong linear correlation. Compared with the previously reported SERS substrates, the enormous SERS enhancing behavior of our proposed SERS platform benefits from the high-density hotspots generated by the strong coupling between surface plasmons in the hybrid system, mainly including the following points: (i) tip-to-tip plasmonic coupling of AuNS; (ii) interparticle coupling between horizontally AuNS with narrow nanogaps on surfaces of GO; (iii) LSPR effect between the adjacent Au@Ag NPs; (iv) plasmonic coupling between GANS NCs and Au@Ag NPs in both horizontal and vertical directions and (v) superior enrichment ability and additional CM of GO. Therefore, our proposed multi-dimensional plasmonic coupling platform provides a new idea for label-free ultrasensitive detection of BR and is hopeful to be expanded to sensitive detection of other biomarkers, which opens up infinite possibilities for clinical diagnosis of various diseases.

CRediT authorship contribution statement

Wenshi Zhao: Conceptualization, Formal analysis, Methodology, Investigation. **Shuo Yang:** Investigation. **Daxin Zhang:** Software. **Tianxiang Zhou:** Validation, Supervision. **Jie Huang:** Software. **Ming Gao:** Validation. **Xiaolong Zhang:** Investigation. **Yang Liu:** Resources, Supervision, Writing – review & editing. **Jinghai Yang:** Resources, Supervision.

Declaration of Competing Interest

The authors declare that they have no known competing financial interests or personal relationships that could have appeared to influence the work reported in this paper.

Data availability

No data was used for the research described in the article.

Acknowledgements

This work was financed by National Natural Science Foundation of China, China (Grant Numbers 21676115), Program for the development of Science and Technology of Jilin province, China (Grant Numbers 20220203021SF, 20200301043RQ and 20200201022JC), Program for Science and Technology of Education Department of Jilin Province, China (Grant Numbers JJKH20210611KJ and JJKH20220444KJ) and Program of Jilin Provincial Development and Reform Commission (Grant Numbers 2021C036-3).

Appendix A. Supplementary data

Supplementary data to this article can be found online at https://doi.org/10.1016/j.jcis.2023.05.117.

References

[1] D. Xu, L. Duan, W. Jia, G. Yang, Y. Gu, Fabrication of Ag@Fe_2O_3 hybrid materials as ultrasensitive SERS substrates for the detection of organic dyes and bilirubin in human blood, Microchem. J. 161 (2021), 105799.
[2] M.E. Avramescu, W.F. Sager, Z. Borneman, M. Wessling, Adsorptive membranes for bilirubin removal, Journal of chromatography B, J. Chromatogr. B 803 (2004) 215–223.
[3] D. Gao, X. Yang, P. Teng, M. Luo, H. Zhang, Z. Liu, et al., On-line SERS detection of bilirubin based on the optofluidic in-fiber integrated GO/Ag NPs for rapid diagnosis of jaundice, Talanta 234 (2021), 122692.
[4] A.D. Kartashova, K.A. Gonchar, D.A. Chermoshentsev, E.A. Alekseeva, M.B. Gongalsky, I.V. Bozhev, et al., Surface-Enhanced Raman Scattering-Active Gold-Decorated Silicon Nanowire Substrates for Label-Free Detection of Bilirubin, ACS Biomater. Sci. Eng. (2021).
[5] L. Ouyang, L. Yao, R. Tang, X. Yang, L. Zhu, Biomimetic point-of-care testing of trace free bilirubin in serum by using glucose selective capture and surface-enhanced Raman spectroscopy, Sensor. Actuat. B-Chem. 340 (2021), 129941.
[6] K. Shanmugaraj, S.A. John, Water-soluble MoS_2 quantum dots as effective fluorescence probe for the determination of bilirubin in human fluids, Spectrochim. Acta A Mol. Biomol. Spectrosc. 215 (2019) 290–296.
[7] Z.-Q. Geng, D. Xu, Y. Song, W.-P. Wang, Y.-P. Li, C.-Q. Han, et al., Sensitive label-free detection of bilirubin in blood using boron nitride-modified nanorod arrays as SERS substrates, Sensor. Actuat. B-Chem. 334 (2021), 129634.
[8] Y. Zou, Y. Zhang, Y. Xu, Y. Chen, S. Huang, Y. Lyu, et al., Portable and Label-Free Detection of Blood Bilirubin with Graphene-Isolated-Au-Nanocrystals Paper Strip, Anal. Chem. 90 (2018) 13687–13694.
[9] X. Pan, L. Li, H. Lin, J. Tan, H. Wang, M. Liao, et al., A graphene oxide-gold nanostar hybrid based-paper biosensor for label-free SERS detection of serum bilirubin for diagnosis of jaundice, Biosens. Bioelectron. 145 (2019), 111713.
[10] Y. Hang, J. Boryczka, N. Wu, Visible-light and near-infrared fluorescence and surface-enhanced Raman scattering point-of-care sensing and bio-imaging: a review, Chem. Soc. Reviews 51 (2022) 329–375.
[11] R. Chikkaraddy, A. Xomalis, L.A. Jakob, J.J. Baumberg, Mid-infrared-perturbed molecular vibrational signatures in plasmonic nanocavities, Light-Sci. Appl. 11 (2022) 19.
[12] Z. Chen, M. Segev, Highlighting photonics: looking into the next decade, eLight 1 (2021) 2.
[13] D. Lee, S. So, G. Hu, M. Kim, T. Badloe, H. Cho, et al., Hyperbolic metamaterials: fusing artificial structures to natural 2D materials, eLight 2 (2022) 1.
[14] S. Yang, J. Yao, Y. Quan, M. Hu, R. Su, M. Gao, et al., Monitoring the charge-transfer process in a Nd-doped semiconductor based on photoluminescence and SERS technology, Light-Sci. Appl. 9 (2020) 117.
[15] J. Xiong, S.-T. Wu, Planar liquid crystal polarization optics for augmented reality and virtual reality: from fundamentals to applications, eLight 1 (2021) 3.
[16] Y. Quan, J. Li, M. Hu, M. Wei, J. Yang, M. Gao, et al., Interface synthesis of MoS_2@ZnO@Ag SERS substrate for the ultrasensitive determination of bilirubin, Appl. Surf. Sci. 598 (2022), 153750.
[17] W. Zhao, D. Zhang, T. Zhou, J. Huang, Y. Wang, B. Li, et al., Aptamer-conjugated magnetic Fe_3O_4@Au core-shell multifunctional nanoprobe: A three-in-one aptasensor for selective capture, sensitive SERS detection and efficient near-infrared light triggered photothermal therapy of Staphylococcus aureus, Sensor. Actuat. B-Chem. 350 (2022), 130879.
[18] A.E. Kandjani, M. Mohammadtaheri, A. Thakkar, S.K. Bhargava, V. Bansal, Zinc oxide/silver nanoarrays as reusable SERS substrates with controllable 'hot-spots' for highly reproducible molecular sensing, J. Colloid Interf. Sci. 436 (2014) 251–257.
[19] T. Cong, J. Wang, Y. Zhao, D. Zhang, Z. Fan, L. Pan, Tip-to-tip assembly of urchin-like Au nanostar at water-oil interface for surface-enhanced Raman spectroscopy detection, Anal. Chim. Acta 1154 (2021), 338323.
[20] L. Xu, Q. Ding, Magnetic field induced high-density SERS active assembly of Fe_3O_4@Au nanostars in a glass capillary for food colorant detection, Anal. Methods 13 (2021) 5487–5492.
[21] H.L. Wang, E.M. You, R. Panneerselvam, S.Y. Ding, Z.Q. Tian, Advances of surface-enhanced Raman and IR spectroscopies: from nano/microstructures to macro-optical design, Light-Sci. Appl. 10 (2021) 161.
[22] A. Basiri, M.Z.E. Rafique, J. Bai, S. Choi, Y. Yao, Ultrafast low-pump fluence all-optical modulation based on graphene-metal hybrid metasurfaces, Light-Sci. Appl. 11 (2022) 102.
[23] H. Shang, M. Ding, X. Zhang, W. Zhang, Dual-mode biosensing platform for sensitive and portable detection of hydrogen sulfide based on cuprous oxide/gold/copper metal organic framework heterojunction, J. Colloid Interf. Sci. 629 (2023) 796–804.
[24] H. Tang, T. Yang, L. Chen, Y. Zhang, Y. Zhu, C. Wang, et al., Surface chemistry of graphene tailoring the activity of digestive enzymes by modulating interfacial molecular interactions, J. Colloid Interf. Sci. 630 (2023) 179–192.
[25] A. Zhang, J. Chang, Y. Chen, Z. Huang, G. Alfranca, Q. Zhang, et al., Spontaneous implantation of gold nanoparticles on graphene oxide for salivary SERS sensing, Anal. Methods 11 (2019) 5089–5097.
[26] L. Liu, S. Hou, X. Zhao, C. Liu, Z. Li, C. Li, et al., Role of Graphene in Constructing Multilayer Plasmonic SERS Substrate with Graphene/AgNPs as Chemical Mechanism-Electromagnetic Mechanism Unit, Nanomaterials 10 (2020) 2371.
[27] R. Liu, Z. Zha, M. Shafi, C. Li, W. Yang, S. Xu, et al., Bulk plasmon polariton in hyperbolic metamaterials excited by multilayer nanoparticles for surface-enhanced Raman scattering (SERS) sensing, Nanophotonics 10 (2021) 2949–2958.
[28] A. Pollap, P. Swit, Recent Advances in Sandwich SERS Immunosensors for Cancer Detection, Int. J. Mol. Sci. 23 (2022) 4740.
[29] T. Wu, H. Zheng, Y. Kou, X. Su, N.R. Kadasala, M. Gao, et al., Self-sustainable and recyclable ternary Au@Cu_2O-Ag nanocomposites: application in ultrasensitive SERS detection and highly efficient photocatalysis of organic dyes under visible light, Microsys. Nanoeng. 7 (2021) 23.
[30] H. Yang, Q. He, M. Lin, L. Ji, L. Zhang, H. Xiao, et al., Multifunctional Au@Pt@Ag NPs with color-photothermal-Raman properties for multimodal lateral flow immunoassay, J. Hazard. Mater. 435 (2022), 129082.
[31] Y.J. Zhang, P.M. Radjenovic, X.S. Zhou, H. Zhang, J.L. Yao, J.F. Li, Plasmonic Core-Shell Nanomaterials and their Applications in Spectroscopies, Adv. Mater. 33 (2021) e2005900.
[32] T. Yaseen, H. Pu, D.-W. Sun, Effects of Ions on Core-Shell Bimetallic Au@Ag NPs for Rapid Detection of Phosalone Residues in Peach by SERS, Food Anal. Methods 12 (2019) 2094–2105.

[33] D.C. Marcano, D.V. Kosynkin, J.M. Berlin, A. Sinitskii, Z. Sun, A. Slesarev, et al., Improved Synthesis of Graphene Oxide, ACS Nano 4 (2010) 4806–4814.
[34] Y. Fang, S. Guo, C. Zhu, Y. Zhai, E. Wang, Self-Assembly of Cationic Polyelectrolyte-Functionalized Graphene Nanosheets and Gold Nanoparticles: A Two-Dimensional Heterostructure for Hydrogen Peroxide Sensing, Langmuir 26 (2010) 11277–11282.
[35] J. Li, J. Wu, X. Zhang, Y. Liu, D. Zhou, H. Sun, et al., Controllable Synthesis of Stable Urchin-like Gold Nanoparticles Using Hydroquinone to Tune the Reactivity of Gold Chloride, J. Phys. Chem. C 115 (2011) 3630–3637.
[36] J. Huang, T. Zhou, H. Zheng, J. Wang, Y. Jiang, Y. Zhang, et al., Construction of ternary multifunctional Fe_3O_4/Cu_2O/Au nanocomposites: SERS detection and visible light driven photocatalysis for organic dyes, Ceram. Int. 48 (2022) 25413–25423.
[37] Y. Kou, T. Wu, H. Zheng, N.R. Kadasala, S. Yang, C. Guo, et al., Recyclable Magnetic MIP-Based SERS Sensors for Selective, Sensitive, and Reliable Detection of Paclobutrazol Residues in Complex Environments, ACS Sustain. Chem. Eng. 8 (2020) 14549–14556.
[38] L. Sun, Z. Yu, M. Lin, Synthesis of polyhedral gold nanostars as surface-enhanced Raman spectroscopy substrates for measurement of thiram in peach juice, Analyst 144 (2019) 4820–4825.
[39] N. Peruffo, F. Mancin, E. Collini, Plexcitonic Nanohybrids Based on Gold Nanourchins: The Role of the Capping Layer, J. Phys. Chem. C 125 (2021) 19897–19905.
[40] M. Liu, C. Zheng, M. Cui, X. Zhang, D.P. Yang, X. Wang, et al., Graphene oxide wrapped with gold nanorods as a tag in a SERS based immunoassay for the hepatitis B surface antigen, Microchim. Acta 185 (2018) 458.
[41] X. Yu, Y. Zhong, Y. Sun, Y. Chen, Controllable Preparation of Plasmonic Gold Nanostars for Enhanced Photothermal and SERS Effects, Chemical Res. Chinese U. 36 (2020) 1284–1291.
[42] Y. Zhang, S. Liu, L. Wang, X. Qin, J. Tian, W. Lu, et al., One-pot green synthesis of Ag nanoparticles-graphene nanocomposites and their applications in SERS, H_2O_2, and glucose sensing, RSC Adv. 2 (2012) 538–545.
[43] W. Zhao, S. Yang, D. Zhang, T. Zhou, J. Huang, M. Gao, et al., Ultrasensitive dual-enhanced sandwich strategy for simultaneous detection of Escherichia coli and Staphylococcus aureus based on optimized aptamers-functionalized magnetic capture probes and graphene oxide-Au nanostars SERS tags, J. Colloid Interf. Sci. 634 (2023) 651–663.
[44] J. Huang, T. Zhou, W. Zhao, S. Cui, R. Guo, D. Li, et al., Multifunctional magnetic Fe_3O_4/Cu_2O-Ag nanocomposites with high sensitivity for SERS detection and efficient visible light-driven photocatalytic degradation of polycyclic aromatic hydrocarbons (PAHs), J. Colloid Interf. Sci. 628 (2022) 315–326.
[45] M. Richard-Lacroix, V. Deckert, Direct molecular-level near-field plasmon and temperature assessment in a single plasmonic hotspot, Light-Sci. Appl. 9 (2020) 35.
[46] Y. Long, W. Wang, W. Xiong, H. Li, Hybrid structure design, preparation of Ag-GO SERS optical fiber probe and its chemical, electromagnetic enhancement mechanism, J. Alloy. Compd. 901 (2022), 163660.
[47] X.-K. Kong, Q.-W. Chen, Z.-Y. Sun, Enhanced SERS of the complex substrate using Au supported on graphene with pyridine and R6G as the probe molecules, Chem. Phys. Lett. 564 (2013) 54–59.
[48] J. Lin, J. Yu, O.U. Akakuru, X. Wang, B. Yuan, T. Chen, et al., Low temperature-boosted high efficiency photo-induced charge transfer for remarkable SERS activity of ZnO nanosheets, Chem. Sci. 11 (2020) 9414–9420.
[49] X.H. Pham, E. Hahm, H.M. Kim, S. Shim, T.H. Kim, D.H. Jeong, et al., Silver Nanoparticle-Embedded Thin Silica-Coated Graphene Oxide as an SERS Substrate, Nanomaterials 6 (2016) 176.
[50] J. He, G. Song, X. Wang, L. Zhou, J. Li, Multifunctional magnetic Fe_3O_4/GO/Ag composite microspheres for SERS detection and catalytic degradation of methylene blue and ciprofloxacin, J. Alloy. Compd. 893 (2022), 162226.
[51] Y. Wang, M. Zhang, H. Yu, Y. Zuo, J. Gao, G. He, et al., Facile fabrication of Ag/graphene oxide/TiO_2 nanorod array as a powerful substrate for photocatalytic degradation and surface-enhanced Raman scattering detection, Appl. Catal. B-Environ. 252 (2019) 174–186.
[52] S.S. Singha, S. Mondal, T.S. Bhattacharya, L. Das, K. Sen, B. Satpati, et al., Au nanoparticles functionalized 3D-MoS_2 nanoflower: An efficient SERS matrix for biomolecule sensing, Biosens. Bioelectron. 119 (2018) 10–17.
[53] S.R. Sahoo, S. Huey-Jen Hsu, D.-A. Chou, G.-J. Wang, C.-C. Chang, Surface plasmon-enhanced fluorescence and surface-enhanced Raman scattering dual-readout chip constructed with silver nanowires: Label-free clinical detection of direct-bilirubin, Biosens. Bioelectron. 213 (2022), 114440.
[54] Y. Mao, B. Yu, H. Zhang, Y. Ma, F. Han, B. Zhou, et al., Surfactant-free preparation expanded graphite coupled with Ag nanoparticles as SERS high sensor via optimizing electromagnetic enhancement and adsorption behavior, Appl. Surf. Sci. 592 (2022), 153264.
[55] Z. Li, X. Huang, K. Wu, Y. Jiao, C. Zhou, Fabrication of regular macro-mesoporous reduced graphene aerogel beads with ultra-high mechanical property for efficient bilirubin adsorption, Mater. Sci. Eng. C-Mater. 106 (2020), 110282.
[56] X. Song, S. Cui, Z. Li, Y. Jiao, C. Zhou, Fabrication of chitin/graphene oxide composite sponges with higher bilirubin adsorption capacity, J. Mater. Sci. Mater. M. 29 (2018) 108.
[57] X. Song, X. Huang, Z. Li, Z. Li, K. Wu, Y. Jiao, et al., Construction of blood compatible chitin/graphene oxide composite aerogel beads for the adsorption of bilirubin, Carbohyd. Polym. 207 (2019) 704–712.
[58] Z. Chen, Y. Sun, J. Shi, W. Zhang, X. Zhang, X. Huang, et al., Facile synthesis of Au@Ag core-shell nanorod with bimetallic synergistic effect for SERS detection of thiabendazole in fruit juice, Food Chem. 370 (2022), 131276.
[59] X. Li, X. Lin, G. Fang, H. Dong, J. Li, S. Cong, et al., Interfacial layer-by-layer self-assembly of PS nanospheres and Au@Ag nanorods for fabrication of broadband and sensitive SERS substrates, J. Colloid Interf. Sci. 620 (2022) 388–398.
[60] Q. Bai, H. Luo, S. Shi, S. Liu, L. Wang, F. Du, et al., AuAg nanocages/graphdiyne for rapid elimination and detection of trace pathogenic bacteria, J. Colloid Interf. Sci. 613 (2022) 376–383.
[61] D.-Z. Zhu, J.-F. Yan, Z.-W. Liang, J.-W. Xie, H.-L. Bai, Laser stripping of Ag shell from Au@Ag nanoparticles, Rare Met. 40 (2021) 3454–3459.
[62] S. Lin, H. Guan, Y. Liu, S. Huang, J. Li, W. Hasi, et al., Binary Plasmonic Assembly Films with Hotspot-Type-Dependent Surface-Enhanced Raman Scattering Properties, ACS Appl. Mater. Inter. 13 (2021) 53289–53299.
[63] C. Xia, Y. Xu, M.M. Cao, Y.P. Liu, J.F. Xia, D.Y. Jiang, et al., A selective and sensitive fluorescent probe for bilirubin in human serum based on europium(III) post-functionalized Zr(IV)-Based MOFs, Talanta 212 (2020), 120795.
[64] Z.-J. Lu, Y. Cheng, Y. Zhang, X. Wang, P. Xu, H. Yu, et al., Non-enzymatic free bilirubin electrochemical sensor based on ceria nanocube, Sensor. Actuat. B-Chem. 329 (2021), 129224.